

2017-08-16

# Aeolian sediment fingerprinting using a Bayesian mixing model

Gholami, H

<http://hdl.handle.net/10026.1/9893>

---

10.1002/esp.4189

Earth Surface Processes and Landforms

Wiley

---

*All content in PEARL is protected by copyright law. Author manuscripts are made available in accordance with publisher policies. Please cite only the published version using the details provided on the item record or document. In the absence of an open licence (e.g. Creative Commons), permissions for further reuse of content should be sought from the publisher or author.*

**Aeolian sediment fingerprinting using a Bayesian mixing model**

Journal:	<i>Earth Surface Processes and Landforms</i>
Manuscript ID	ESP-17-0002.R1
Wiley - Manuscript type:	Research Article
Date Submitted by the Author:	n/a
Complete List of Authors:	Gholami, Hamid; University of Hormozgan, Department of Range and Watershed Management Telfer, Matt; Plymouth University, School of Geography, Earth and Environmental Sciences Blake, William; Plymouth University, SoGEES Fathabadi, Abolhassan; University of Gonbad-e-Kavoos, Department of Range and Watershed Management
Keywords:	Aeolian sediment, Sand provenance, Markov Chain Monte Carlo, Fingerprinting, Dune

SCHOLARONE™  
Manuscripts

# 1 **Aeolian sediment fingerprinting using a Bayesian mixing model**

2  
3 Hamid Gholami <sup>a\*</sup>, Matt W. Telfer <sup>b\*</sup>, William H. Blake <sup>b</sup> and Abolhassan Fathabadi <sup>c</sup>

4 <sup>a</sup> Department of Range and Watershed Management, University of Hormozgan,  
5 Bandar-Abbas, Hormozgan, Iran.

6 <sup>b</sup> School of Geography, Earth and Environmental Sciences, Plymouth University,  
7 Plymouth, Devon, PL4 8AA , UK.

8 <sup>c</sup> Department of Range and Watershed Management, University of Gonbad-e-  
9 Kavoos, Gonbad-e-Kavoos, Golestan, Iran.

10 \* Correspondence to:

11 Hamid Gholami, Department of Range and Watershed Management, University of  
12 Hormozgan, Bandar-Abbas, Hormozgan, Iran. *E-mail address:*  
13 hgholami@hormozgan.ac.ir. Tel: +98 937 0865077.

14 and

15 Matt Telfer, School of Geography, Earth and Environmental Science, Plymouth  
16 University, Plymouth, Devon, PL4 8AA, UK. *E-mail address:*  
17 matt.telfer@plymouth.ac.uk. Tel: +44 1752 585570.

## 18 19 **Abstract**

20 Identifying sand provenance in depositional aeolian environments (e.g. dunefields)  
21 can elucidate sediment pathways and fluxes, and inform potential land management  
22 strategies where windblown sand and dust is a hazard to health and infrastructure.

1  
2  
3 23 However, the complexity of these pathways typically makes this a challenging  
4  
5 24 proposition, and uncertainties on the composition of mixed-source sediments are  
6  
7 25 often not reported. This study demonstrates that a quantitative fingerprinting method  
8  
9  
10 26 within the Bayesian Markov Chain Monte Carlo (MCMC) framework offers great  
11  
12 27 potential for exploring the provenance and uncertainties associated with aeolian  
13  
14 28 sands.

15  
16 29 Eight samples were taken from dunes of the small (~58 km<sup>2</sup>) Ashkzar erg, central  
17  
18 30 Iran, and forty-nine from three distinct potential sediment sources from the  
19  
20  
21 31 surrounding area. These were analyzed for 61 tracers including 53 geochemical  
22  
23 32 elements (trace, major and rare earth elements (REE)) and 8 REE ratios. Kruskal–  
24  
25 33 Wallis H-tests and stepwise discriminant function analysis (DFA) allowed the  
26  
27 34 identification of an optimum composite fingerprint based on six tracers (Rb, Sr, <sup>87</sup>Sr,  
28  
29 35 (La/Yb)<sub>n</sub>, Ga and δCe), and a Bayesian mixing model was applied to derive the  
30  
31 36 source apportionment estimates within an uncertainty framework.

32  
33  
34 37 There is substantial variation in the uncertainties in the fingerprinting results, with  
35  
36 38 some samples yielding clear discrimination of components, and some with less clear  
37  
38 39 fingerprints. Quaternary terraces and fans contribute the largest component to the  
39  
40 40 dunes, but they are also the most extensive surrounding unit; clay flats and marls,  
41  
42 41 however, contribute out of proportion to their small outcrop extent. The successful  
43  
44 42 application of these methods to aeolian sediment deposits demonstrates their  
45  
46 43 potential for providing quantitative estimates of aeolian sediment provenances in  
47  
48 44 other mixed-source arid settings, and may prove especially beneficial where  
49  
50 45 sediment is derived from multiple sources, or where other methods of provenance  
51  
52 46 (e.g. detrital zircon U-Pb dating) are not possible due to mineralogical constraints.  
53  
54  
55  
56  
57  
58  
59  
60

1  
2  
3  
4  
5  
6  
7  
8  
9  
10  
11  
12  
13  
14  
15  
16  
17  
18  
19  
20  
21  
22  
23  
24  
25  
26  
27  
28  
29  
30  
31  
32  
33  
34  
35  
36  
37  
38  
39  
40  
41  
42  
43  
44  
45  
46  
47  
48  
49  
50  
51  
52  
53  
54  
55  
56  
57  
58  
59  
60

47 **Key words:** Sand provenance; Aeolian sediment; Markov Chain Monte Carlo;  
48 Fingerprinting; uncertainty.

For Peer Review

## 1. Introduction

Identifying and quantifying the source(s) of aeolian sediments is a long-standing challenge for geoscientists, and yet such information is often of crucial importance in understanding sediment fluxes at a range of scales. As well as providing fundamental knowledge on long-term landscape evolution (e.g. Pell et al., 1997), aeolian provenance studies have been used to elucidate past wind regimes and palaeoclimates (e.g. Nanson et al., 1995), investigate hazardous dust transport pathways (e.g. Pethierick et al., 2008; Yang et al., 2007) and inform studies of the palaeoclimatic record of the Antarctic ice-core dust record (Delmonte et al., 2010; Delmonte et al., 2004). The challenges with the task arise not just from the diverse range of potential sources for aeolian sands and dusts (e.g. geological or lithological units, soil units, land use types and geomorphological landscapes), and the long transport distances which may be involved (on the order of  $10\text{-}10^2$  km for aeolian sand and  $10\text{-}10^3$  km for aeolian dust), but also the potential complexity of transport pathways (Huntsman-Mapila et al., 2005). Before deposition at its current location, an aeolian sand grain may have been through multiple cycles of fluvial, aeolian, lacustrine and/or colluvial deposition and subsequent mobilization. Aeolian sands, therefore, rarely retain an easy-to-interpret signature of their origins.

The use of geochemical fingerprinting methods to determine sediment provenance has progressively increased since the late 1990s (Walling, 2013). Application has been focused most widely in fluvial contexts (Haddadchi et al 2013) wherein there recent work has highlighted the need to pay attention to challenges in signature development and tracer behavior (Koiter et al., 2013). Sediment fingerprinting involves the identification, quantification and statistical testing of a range of source

1  
2  
3 74 material properties capable of discriminating between potential sediment sources  
4  
5 75 with a view to improving knowledge of sediment source and transport processes  
6  
7 76 (Collins et al., 2017) . These properties may include geochemical characteristics  
8  
9 77 (e.g. Douglas et al., 2009; Lin et al., 2015), radionuclide concentrations (Wilson et  
10  
11 78 al., 2012), mineralogy (Pittam et al., 2009), geochronological data (principally U-Pb  
12  
13 79 dating of detrital zircons; e.g. Pell et al., 1997; Garzanti et al., 2013), biomarkers  
14  
15 80 (Chen et al., 2016) and colour properties (Martínez-carreras et al., 2010). Although  
16  
17 81 sediment fingerprinting studies of aeolian sands are not new (e.g. Pell et al., 1997;  
18  
19 82 Wasklewicz and Meek, 1995; Winspear and Pye, 1996; Liu et al., 2016; Muhs et al,  
20  
21 83 2017), challenges remain in adequately capturing the uncertainties associated with  
22  
23 84 the diverse sources and pathways that may exist, and adoption of techniques  
24  
25 85 developed in different disciplines offer a route forward. It is noteworthy that in a  
26  
27 86 recent review discussing applications of sediment source-tracing methods (Owens et  
28  
29 87 al., 2016), mention of aeolian sedimentation is limited to health science studies of  
30  
31 88 PM2.5 and PM10 material. The opportunity to utilize these approaches in aeolian  
32  
33 89 process science remains largely overlooked.  
34  
35  
36  
37  
38  
39  
40  
41  
42  
43  
44  
45  
46  
47  
48  
49  
50  
51  
52  
53  
54  
55  
56  
57  
58  
59  
60

90

91 In recent years, increasing attention has been directed to the uncertainty of the  
92 results generated by sediment source fingerprinting. It is important that such  
93 uncertainty is recognized, particularly if the results are to be used to target  
94 investment in sediment control measures (Mukundan et al., 2012). The factors  
95 contributing to uncertainty in estimates of source apportionment are manifold and  
96 diverse, and have been reviewed elsewhere (e.g. Walling 2010; Koiter et al., 2013;  
97 Collins et al, 2017); here we consider some of the differences between the fluvial  
98 setting of most sediment fingerprinting studies, and the aeolian context considered

1  
2  
3 99 here. Many uncertainties remain the same – for instance, instrumental precision.  
4  
5 100 Other aspects of the aeolian entrainment, transport and depositional system,  
6  
7 101 however, differ markedly from fluvial settings. Due to dominance of gravity in  
8  
9 102 controlling - and directing - slope and fluvial processes, and the (usually) confined  
10  
11 103 nature of fluvial systems, erosion and entrainment of sediment from catchments is  
12  
13 104 highly directionally-controlled. In an aeolian context, there is more scope for spatially  
14  
15 105 extensive direct entrainment of sediment, and also more potential for directional  
16  
17 106 variability, and this complex mixing environment may in turn lead to increased  
18  
19 107 covariance between properties used to derive the fingerprint. In addition, such  
20  
21 108 complexities cannot be considered static, as variations in wind regimes over long  
22  
23 109 timescales may lead to changes in these pathways.  
24  
25  
26  
27  
28

29  
30 111 In order to quantify the uncertainty associated to mixing models related to this  
31  
32 112 inherent variability in the source area and sediment mixture data, some recent  
33  
34 113 studies have explored the use of Monte Carlo simulations (e.g. Motha et al., 2003;  
35  
36 114 Collins et al., 2013; Collins et al., 2012; Stone et al., 2014; Smith & Blake, 2014;  
37  
38 115 Sherriff et al., 2015; Vale et al., 2016; Gellis & Noe, 2013; Voli et al., 2013; Wilkinson  
39  
40 116 et al., 2013; Walling et al., 2008). More recently, Bayesian mixing models being  
41  
42 117 employed more comprehensively translate component uncertainties into source  
43  
44 118 apportionment results (Cooper and Krueger, 2017) with several examples  
45  
46 119 undertaken in hydrological contexts (e.g. Fox & Papanicolaou, 2008; Cooper et  
47  
48 120 al., 2014; Cooper et al., 2015; Nosrati et al., 2014; Stewart et al., 2015). To date,  
49  
50 121 however, such approaches have not been used within aeolian sedimentary contexts.  
51  
52  
53

54 122  
55  
56  
57  
58  
59  
60



1  
2  
3 123 The sophistication of aeolian sediment provenance studies currently lags those in  
4  
5 124 the fluvial sphere, and the main aim of this paper is to demonstrate the viability of  
6  
7 125 fingerprinting methods for aeolian sediments, including the estimation of uncertainty,  
8  
9 126 associated with the contributions from different geological units as potential sources  
10  
11 127 for a small dunefield, Ashkzar Erg, in the Yazd-Ardekan Plain, central Iran, using a  
12  
13 128 Bayesian mixing model. Ashkzar erg and its surrounding potential sources cause  
14  
15 129 many serious problems related to wind erosion and associated on-site and off-site  
16  
17 130 effects, with potential impacts on the health of the occupants of the neighbouring city  
18  
19 131 of Yazd (Naddafi et al., 2006). Aeolian deflation is a major erosional process on the  
20  
21 132 Yazd-Ardekan Plain and large amounts of aeolian sediment are often transported to  
22  
23 133 residential regions by wind (Amiraslani and Dragovich, 2011). Therefore, quantifying  
24  
25 134 sediment source contributions to the Ashkzar sand dunes could help to select the  
26  
27 135 best management strategies at this location and others similarly affected by aeolian  
28  
29 136 erosion. Additionally, the findings are considered in their geomorphological context  
30  
31 137 with the aim of explaining the spatial variability in sediment provenance observed at  
32  
33 138 Ashkzar erg.  
34  
35  
36  
37  
38  
39  
40

139

## 140 **2. Materials and methods**

### 141 *2.1. Field location*

142 Yazd-Ardekan (31°10'–32°43' N, 53°68'–54°47' E) is an arid plain in central Iran,  
143 and includes different geomorphic landscapes, such as the Ashkzar and Yazd ergs  
144 (Figure 1). The Yazd-Ardekan Plain is surrounded by mountain ranges. These are  
145 Shirkooch in the south, Ahangaran and the Margh Zard Mountains in the west, Haft  
146 Adamin and Khoonzad Mountains in the east and Chak Chak Mountain in the north.  
147 The area of the plain is ~2900 km<sup>2</sup>, and it consists of 78% Quaternary alluvial fans

1  
2  
3 148 and terraces (Qt<sub>2</sub> geological unit), 13% clay flats (Qc geological unit), 7% Eocene  
4  
5 149 gypsiferous marl (Egm geological unit) and 2% sand dunes (Qsd geological unit)  
6  
7 150 (Figure 1 and 2). About 93% of Yazd-Ardekan Plain is thus covered by Quaternary  
8  
9 151 deposits. Active and stabilized sand dunes in the Ashkzar erg occupy 58 km<sup>2</sup>  
10  
11 152 (centred on 32° 1'N, 54° 10'E), which is dominated by barchans and transverse  
12  
13 153 barchanoid ridges (Figure 2). The erg has a sparse but extensive cover of *Haloxylon*  
14  
15 154 *persicum*, a species which is both endemic to the region, and is also used to stabilize  
16  
17 155 mobile sand (Amiraslani and Dragovich, 2011). Based on 50 years of climate data at  
18  
19 156 Yazd Meteorological Station, minimum and maximum annual temperatures are -16  
20  
21 157 °C and 46 °C, respectively. Long-term mean rainfall and annual evaporation in the  
22  
23 158 study area are ~60 mm/year and ~3500 mm/year respectively. According to annual  
24  
25 159 wind roses, dominant winds on the Yazd-Ardekan Plain are mainly from the north  
26  
27 160 and west (Figure 1C).  
28  
29  
30  
31

32 161

33  
34 162 [Approx. location of Figure 1]  
35

36 163

### 37 164 2.2. Sampling and laboratory analysis

38  
39 165 The geological units that were identified as potential sources for sand dunes (Qsd  
40  
41 166 formation) are the Qt<sub>2</sub> (Quaternary alluvial fans and terraces), Qc (Quaternary clay  
42  
43 167 pans and flats) and Egm (Eocene marls) formations. Other surrounding lithologies in  
44  
45 168 the vicinity are hard, igneous exposures and can be discounted from generating  
46  
47 169 substantial quantities of deflatable sediment. In this study, spatially distributed  
48  
49 170 source samples were taken from 49 sites, covering the Egm (n=8), Qc (n=18) and  
50  
51 171 Qt<sub>2</sub> (n=23) potential sources, and eight sediment samples were collected from the  
52  
53 172 Ashkzar sand dunes (Figure 1D). Samples were collected from the upper 0–5 cm  
54  
55  
56  
57  
58  
59  
60

1  
2  
3 173 depth of potential sources (that is, the layer of the regolith exposed to current aeolian  
4  
5 174 entrainment) and sand dunes (that is, the layer of the regolith most recently  
6  
7 175 deposited); this is similar to sampling strategies employed by other provenance  
8  
9 176 studies of aeolian dunes (e.g. Pell et al., 1997), and is accordance with common  
10  
11 177 earth science protocols (Owens et al., 2016). Within each source area, sample  
12  
13 178 selection was based upon locations that were: a) clearly derived from the geological  
14  
15 179 unit in question, b) selected to ensure broad spatial coverage of the source area, and  
16  
17 180 c) clearly influenced by aeolian erosion (e.g. the presence of deflatable unvegetated  
18  
19 181 sand surfaces with ripples, as well as yardangs of a range of scales). Samples  
20  
21 182 numbers were chosen to ensure a balance between the greater spatial extent of the  
22  
23 183 Qt2 unit (i.e. sampling was stratified), whilst maintaining a minimum of eight samples  
24  
25 184 for the smaller Egm and Qc units. The spatial location of sampling sites is shown in  
26  
27 185 Figure 1D.  
28  
29  
30  
31

32 186 All sand dune and potential source samples were dry sieved for particle size data,  
33  
34 187 and to isolate the 62.5-150  $\mu\text{m}$  fraction for further geochemical analysis. This fraction  
35  
36 188 was chosen as it represents the dominant fraction in each of the dune samples  
37  
38 189 (Table 1), and is of a size range susceptible to aeolian transport (whilst excluding  
39  
40 190 any contribution of larger grains from local sources, either by aeolian creep or other  
41  
42 191 transport processes). Concentrations of elements including major, trace and rare  
43  
44 192 earth elements (REE) were determined using ICP-MS, after direct digestion with  
45  
46 193 aqua regia (e.g. Collins et al., 2010; Collins et al., 2012); and concentration of  
47  
48 194 strontium and neodymium isotopes measured by ICP-MS, after digestion with a  
49  
50 195 mixture of  $\text{HNO}_3+\text{HClO}_4+\text{HF}$  (3:2:1) (e.g. Honda et al., 2004; Rao et al., 2011). The  
51  
52 196 relative standard deviation (%RSD), based on three replicates for each determinant  
53  
54 197 on each sample, was consistently  $\leq 4\%$ . With regards to REE concentrations, eight  
55  
56  
57  
58  
59  
60

1  
2  
3 198 REE ratios including  $\Sigma$ REE, Nd/Yb, Eu/Eu\* (Europium Anomaly), (La/Lu)<sub>n</sub>, (La/Sm)<sub>n</sub>,  
4  
5 199 (Gd/Yb)<sub>n</sub>, (La/Yb)<sub>n</sub> and  $\delta$ Ce (Cerium Anomaly) were calculated (e.g. Daga et al.,  
6  
7 200 2008; Dou et al., 2010; Rao et al., 2011). In total, 61 tracers were used to fingerprint  
8  
9 201 the sediments of the Yazd-Ardekan Plain.  
10  
11  
12 202

13  
14 203 [Approx. location of Table 1]  
15

16 204 [Approx. location of Figure 2]  
17

18 205 [Approx. location of Figure 3]  
19

20  
21 206

### 22 207 *2.3. Discrimination of aeolian sediment sources*

23  
24  
25 208 We employed a two-stage statistical method proposed by Collins and Walling (2007)  
26  
27 209 to characterize the composite fingerprint for the sources of the sands of the Ashkzar  
28  
29 210 dunes. In stage one, all individual fingerprint properties were tested for their ability to  
30  
31 211 distinguish source types, using the Kruskal–Wallis H-test. Properties with critical  
32  
33 212 values at the 95% level of confidence could be used in a composite fingerprinting  
34  
35 213 model to discriminate between sources types. In stage two, stepwise discriminant  
36  
37 214 function analysis (DFA) was employed to identify the optimum composite fingerprint  
38  
39 215 model from the properties selected in stage one. The stepwise DFA was based on  
40  
41 216 the minimization of Wilk's lambda was used to select optimum composite fingerprint.  
42  
43 217 The F values were used as the test criteria to enter and remove elements. The  
44  
45 218 threshold of F value for entering and removing of elements was set to 3.84 and 2.71,  
46  
47 219 respectively (e.g. Vale et al, 2016).  
48  
49  
50

### 51 220 *2.4. Bayesian mixing model*

52  
53  
54  
55  
56  
57  
58  
59  
60

221 End-member mixing models have been taken a variety of approaches to account for  
 222 uncertainty in the mixing model (Cooper and Krueger, 2017) and some (e.g. Brewer  
 223 et al., 2005; Fox & Papanicolaou, 2008) have adopted hierarchical Bayesian models,  
 224 which we adopt here. Within the mixing model formulation, we assume that, for each  
 225 source  $s$ , the sample  $i$  tracer composition,  $x$ , has a multivariate normal distribution as  
 226 follows:

$$227 \quad x_s^i \sim \text{MVN}_A(\mu_s, \Sigma_s), \quad s = 1, \dots, N, \quad i = 1, \dots, n_{x,s} \quad (\text{eq. 1})$$

228 where  $n_{x,s}$  indicates the number of samples of source  $s$ ;  $\mu_s$  is a  $A$ -dimensional vector  
 229 representing mean fingerprints for source  $s$ ;  $\Sigma_s$  represents a  $(A \times A)$  dimensional  
 230 covariance matrix for source  $s$ . There are  $n_z$  sediment samples for which  $A$   
 231 fingerprints were measured for each sample  $Z^j = (z_1^j, \dots, z_A^j)^T, j = 1, \dots, n_z$  and these  
 232 fingerprints have multivariate normal distributions:

$$233 \quad Z^j \sim \text{MVN}_A(\mu_j^z, \Sigma^z) \quad (\text{eq. 2})$$

234 Each source  $s$  has a fractional contribution  $p_s^j$  to each sediment sample  $j$ . The  
 235 contribution of source types for each sediment sample is equal to  $p_s^j y_s^j$ , where  $y_s^j$  is  
 236 an unobserved (latent) variable that follow the same distribution as  $X_s^i$ .

$$237 \quad \mu_j^z = \sum_{s=1}^N p_s^j y_s^j, \quad j = 1, \dots, n_z \quad (\text{eq. 3})$$

$$238 \quad \sum_{s=1}^N p_s^j = 1, \quad 0 \leq p_s^j \leq 1 \quad (\text{eq. 4})$$

239 Each fractional contribution must be between zero and one, positive and all of them  
 240 must sum to unity. To meet this constraint, some studies have used Dirichlet  
 241 distribution as a prior for the fractional contribution (e.g. Fox & Papanicolaou, 2008;  
 242 Massoudiehet al., 2013), whereas other studies used transformation such as

1  
2  
3 243 centered log-ratio (CLR) (Semmenset al., 2009), isometric log-ratio (ILR) (e.g.  
4  
5 244 Cooper et al., 2015; Parnell et al., 2013; Egozcue et al., 2003) and additive log-ratio  
6  
7 245 (ALR) (e.g. Brewer et al., 2005; Palmer & Douglas, 2008). In this study, a CLR  
8  
9  
10 246 transformation was used, as it has been shown to produce comparable median  
11  
12 247 values to other methods, but with better precision (Cooper et al., 2014). The  
13  
14 248 transformation applied is thus:

$$17 \quad 249 \quad \phi_i = CLR(P_i) = \log\left[\frac{P_{i1}}{g(P_i)}, \dots, \frac{P_{ik}}{g(P_i)}\right] \quad (\text{eq. 5})$$

$$20 \quad 250 \quad \phi_i \sim (\mu_\phi, \tau_\phi) \quad (\text{eq. 6})$$

21  
22  
23  
24 251 where  $g(p_i)$  is the geometric mean of the proportion vector. Figure 4 shows a  
25  
26 252 directed acyclic graph of the model. Compared to an empirical Bayesian approach  
27  
28 253 in which some prior parameters are estimated using deterministic data, the full  
29  
30 254 Bayesian approach employed here needs to specify prior distribution for all  
31  
32  
33 255 parameters. When there is little information about the parameters, using informative  
34  
35 256 hyper-parameters cause biased results. In this study, weakly or non-informative  
36  
37 257 hyper-parameters were used. Multivariate normal and inverse-Wishart distributions  
38  
39 258 were selected as prior distribution for sources means and covariance matrix,  
40  
41 259 respectively.

$$44 \quad 260 \quad \mu_s^X \sim MVN(\theta_s, \tau_s^{-1}), \quad s = 1, \dots, N \quad (\text{eq.7})$$

$$47 \quad 261 \quad \Sigma_s^X \sim Inverse - Wishart(\Omega_s^X, \rho_s^X), \quad s = 1, \dots, N \quad (\text{eq.8})$$

50  
51 262 Here, the hyper-parameter  $\theta_s$  was set to the sample means of the fingerprints and  
52  
53 263  $\tau_s$  was set as a diagonal matrix with values 0.01 on the diagonal. For Wishart  
54  
55  
56 264 distribution, the hyper-parameter  $\Omega_s^X$  is a diagonal matrix with value 1 as diagonal  
57  
58  
59  
60

265 elements and  $\rho_S^X$  was set to six (to reflect the lack of information on the precision  
 266 matrices, and the number of tracers selected for the fingerprint). Similar prior  
 267 distribution and hyper-parameters was assigned for sediment covariance matrix.

$$268 \quad \Sigma^Z \sim \text{Inverse} - \text{Wishart}(\Omega, \rho) \quad (\text{eq.9})$$

269 Weakly informative hyper-parameters  $N(0,1)$  and  $\text{Inv-}\Gamma(2,1)$  were assigned for  
 270  $\mu_\phi$  and  $\tau_\phi$ , respectively.

271 The complete posterior distribution of all model parameters for sediment sample  $Z_j$   
 272 can thus be written as

$$273 \quad (\Sigma_S, \tau_\phi, \mu_\phi, \Sigma^Z, p_j, \phi, \mu_S | X, Z_j) \propto \prod_{S=1}^N \prod_{i=1}^{n_{x,s}} \{P(x_s^i | \mu_S, \Sigma_S)\} \times \prod_{S=1}^N P(\mu_S | \theta_S, \tau_S^{-1}) \times$$

$$274 \quad \prod_{S=1}^N P(\Sigma_S | \Omega_S, \rho_S) \times P(Z_j | \mu_j^Z, \Sigma^Z) \times P(\Sigma^Z | \Omega, \rho) \times P(\phi | \mu_\phi, \tau_\phi) \times P(\mu_\phi) \times P(\tau_\phi)$$

$$275 \quad (\text{eq.10})$$

276 As the joint posterior of all parameters is complex and high-dimensional, we cannot  
 277 directly obtain posterior distribution functions, but the Bayesian model thus defined  
 278 can be analyzed using Markov Chain Monte Carlo (MCMC); we have used the  
 279 WinBUGS package (Lunn et al., 2000) to derive parameter estimates. MCMC  
 280 methods require that the chain reaches a steady state, and the number of runs  
 281 required to reach this state is considered as burn in. The model was run by taking  
 282 50,000,000 times from the posterior distribution from the sand dune and source  
 283 samples, and the first 5,000,000 runs were considered as burn in. The large number  
 284 of iterations was used to ensure convergence, despite the model's complexity and  
 285 high dimensionality; the model converged during the run, as assessed by trace plots  
 286 of simulations, Monte Carlo error and autocorrelation.

287

1  
2  
3 288 [Approx. location of Figure 4]  
4  
5  
6

7  
8  
9 289

### 10 290 **3. Results**

11 291 Grain size data are presented in Table 1 to enable consideration of potential sorting  
12 292 effects during aeolian transportation. The sources reveal very similar physical grain  
13 293 sizes, and it is worth noting that whilst the Qc unit is mapped as a 'clay flat', the  
14 294 sediment sampled for analysis is dominantly sand. The erg, on the other hand, as  
15 295 might be expected as a result of aeolian transport and deposition is better sorted,  
16 296 and less enriched in the coarse and very coarse sand fraction. The individual dune  
17 297 sand samples retain marked variability, with the very-fine (62.5-150  $\mu\text{m}$ ) fraction  
18 298 ranging from 37% to 65%, and a single sample (8) retaining a substantial coarse (>  
19 299 600  $\mu\text{m}$ ) component.  
20  
21  
22  
23  
24  
25  
26  
27  
28  
29

30 300

31  
32 301 The Kruskal-Wallis H test (i.e. one-way ANOVA) was performed on geological units  
33 302 Egm, Qc and Qt2. Results identified 25 significant tracers between these groups  
34 303 (Table 2). Tracers that failed this test ( $p > 0.05$ ) were removed. These were: Nd, Sm,  
35 304 Gd, Tb, Dy, Yb, Lu, (Nd/Yb), (Gd/Yb)<sub>n</sub>, (La/Sm)<sub>n</sub>, V, Cr, Co, Ni, Cu, Zn, Y, Zr, Nb, Ta,  
36 305 U, As, Bi, Cd, Ge, In, Mo, Sb, Se, Te, W, Mn, Si, <sup>143</sup>Nd, <sup>144</sup>Nd and <sup>86</sup>Sr. Whilst the  
37 306 successful discrimination of different tracers between geological units will vary when  
38 307 this method is applied to settings other than this location, the presence of 25 tracers  
39 308 with significant discriminatory power suggests that this method may be applicable in  
40 309 diverse geological settings and/or areas with contrasting weathering regimes.  
41  
42  
43  
44  
45  
46  
47  
48  
49  
50

51 310

52  
53  
54 311 [Approx. location of Table 2]  
55  
56  
57  
58  
59  
60

312



1  
2  
3 313 According to the DFA, a total of six individual tracer properties (Rb, Sr, <sup>87</sup>Sr,  
4  
5 314 (La/Yb)<sub>n</sub>, Ga and δCe) were selected for the optimum composite fingerprint, which  
6  
7 315 correctly discriminated 81.6% of the source type samples (Figure 5).  
8  
9

10 316

11 317 [Approx. location of Table 3]

12  
13 318 [Approx. location of Figure 5]  
14  
15

16 319

17 320 Although DFA results suggested that good source discrimination was achieved, with  
18  
19 321 clear separation of the three group centroids, samples sourced from Qc were found  
20  
21 322 to slightly overlap with the Qt2 source when the first two discriminant functions were  
22  
23 323 plotted, and, to a lesser degree Qt2 and Egm also overlap slightly (Figure 5). The  
24  
25 324 mean and SD of six optimum composite fingerprints that were selected for the  
26  
27 325 Bayesian mixing model, are presented in Table 3. These were tested for normality  
28  
29 326 via Wilks-Shapiro tests (Table 4), and the raw data revealed that the Sr and δCe  
30  
31 327 tracers did not follow a normal distribution for all settings. To account for this, Box-  
32  
33 328 Cox transformations (Box and Cox, 1964) were applied to all data, and the  
34  
35 329 transformed data were used for model experimentation.  
36  
37  
38  
39

40 330

41 331 [Approx. location of Table 4]  
42  
43

44 332

45  
46 333 The derived source contributions for the eight sand dune samples are presented in  
47  
48 334 Table 5 and Figure 6. Overall, the alluvial fans and terraces (Qt2) provide the most  
49  
50 335 abundant supply of sands (mean contribution across all 8 samples = 45.4%, and  
51  
52 336 locally up to 92.7%), with the clay pans (Qc) and Eocene marls (Egm) each  
53  
54 337 contributing around a quarter of the net sediment aeolian flux. However, the  
55  
56 338 composition of the dune sands is highly variable, with different samples dominated  
57  
58  
59  
60

1  
2  
3 339 by different contributing sources, and locally, all three of the potential sources occur  
4  
5 340 as both maxima and minima.  
6

7 341

8  
9 342 [Approx. location of Figure 6]  
10

11  
12 343

#### 13 14 344 **4. Discussion**

##### 15 16 17 345 4.1 Development of a Bayesian mixing model to discriminate aeolian sediment 18 19 346 pathways

20  
21  
22  
23 347 The mixing model to fingerprint aeolian sediment sources deployed in this study  
24  
25 348 used composite signature comprising a suite of six geochemical characteristics (Rb,  
26  
27 349 Sr,  $^{87}\text{Sr}$ , La:Yb, Ga and  $\delta\text{Ce}$ ) identified by stepwise DFA as the most appropriate,  
28  
29 350 and was able to account for >82% of the variance between the three sources. The  
30  
31 351 suite of properties selected by the DFA method most likely reflects two principal  
32  
33 352 factors; the ultimate source of the sediments, and the degree of weathering. The  
34  
35 353 latter might well have variable influence across the source areas, and hence there is  
36  
37 354 some overlap between samples of each class. High La:Yb ratios, for instance, are  
38  
39 355 typically associated with deep igneous lithogenesis (Deffant and Drummond, 1990)  
40  
41 356 and may locally reflect differing sediment contributions from the Precambrian  
42  
43 357 crystalline basement provinces of central Iran.  $\delta\text{Ce}$ , similarly, is often associated with  
44  
45 358 intrusive igneous rocks, although may also be enriched in some sedimentary rocks  
46  
47 359 (Wedepohl, 1978); in this study, the highest concentrations are found in the alluvial  
48  
49 360 fans derived from the adjacent igneous mountains, but the second highest  
50  
51 361 concentrations are found in the sedimentary marls of the Egm unit (Figure 2). In  
52  
53 362 short, the highly varied geology of central Iran, ranging from Precambrian magmatic  
54  
55  
56  
57  
58  
59  
60

1  
2  
3 363 rocks to Cenozoic marine sediments, promotes a high degree of variance in the  
4  
5 364 geochemical fingerprint of modern aeolian sediments. Compounding this is the range  
6  
7 365 of weathering intensities seen, from the intense weathering history of the sediments  
8  
9 366 of Quaternary clay pans, to the more moderate weathering of the sands of the  
10  
11 367 alluvial fans forming the piedmonts of the neighbouring ranges.

12  
13  
14  
15 368 4.2 Potential for application to other aeolian depositional settings

16  
17  
18 369 Despite the usefulness of understanding the provenance of aeolian sands, the  
19  
20 370 sophistication of unmixing models within the aeolian science community generally  
21  
22 371 lags that of fluvial science, in particular in terms of the numerical underpinning of  
23  
24 372 methods applied. Indeed, many such studies attempt to derive provenance estimates  
25  
26 373 only qualitatively (e.g. Fitzsimmons et al, 2009), or, in the few recent cases where  
27  
28 374 robust unmixing models have been applied, relatively simple approaches to  
29  
30 375 incorporating uncertainty into models have been taken (e.g. Liu et al., 2016).

31  
32  
33  
34 376 The successful application of a Bayesian model within an MCMC framework to  
35  
36 377 aeolian sands of a small erg in this study demonstrates the potential of this approach  
37  
38 378 more widely. It is particularly likely to complement detrital zircon U-Pb dating  
39  
40 379 provenance studies, and may prove especially useful in settings where there are  
41  
42 380 insufficient zircon grains to enable the application of this method (e.g. Jia et al.,  
43  
44 381 2015, Nie and Peng, 2014, Ren et al., 2014, Thorpe et al., 1992). Further application  
45  
46 382 of the methods demonstrated here is required to test the ability of such methods  
47  
48 383 globally, but these results suggest a promising future, and a new direction for aeolian  
49  
50 384 provenance studies. For instance, it would be useful to explore the power of these  
51  
52 385 methods in larger-scale settings, such as the continental dunefields of southern  
53  
54 386 Africa and Australia, where provenance studies have been used to explore the  
55  
56  
57  
58  
59  
60

1  
2  
3 387 relationship between tectonic setting and sedimentation (e.g. Garzanti et al., 2014)  
4  
5 388 and explore the long-term evolution of landscapes (e.g. Pell et al., 1997; 2000). This  
6  
7 389 will also elucidate the importance of diversity of local geology and weathering  
8  
9 390 regimes in producing sufficiently distinctive fingerprints.

11  
12 391 Accurate propagation of the uncertainties associated with the component  
13  
14 392 contributions is also a valuable aspect of the methodology employed here and allows  
15  
16 393 more realistic interpretation of the data. For instance, the most abundant two source  
17  
18 394 components of samples E (Qt2 = 62.3%; Qc = 23%) and D (Egm = 56.3%; Qc =  
19  
20 395 28.7%) might suggest similar proportions of the major components at these dunes;  
21  
22 396 roughly 60:25. However, consideration of the lower confidence of the fingerprint of  
23  
24 397 sample D (Figure 6) reveals that whilst the composition of this sample is much more  
25  
26 398 open to interpretation, sample E is quite clearly dominated by the alluvial fan-derived  
27  
28 399 sands (Qt2).

30  
31  
32  
33  
34 400

#### 35 36 401 4.3 Implications for aeolian sediment transport pathways

37  
38  
39 402 Overall, the surrounding Quaternary fans and terraces contribute most (~45%) to the  
40  
41 403 composition of Ashkzar erg; yet this is a disproportionately low value, given that they  
42  
43 404 represent 78% of the surrounding area. Conversely, the size of the overall  
44  
45 405 contributions from the Quaternary clay flats (~26%) and Eocene marls (~28%) to the  
46  
47 406 samples studied reveals the importance of these landscape units as sediment  
48  
49 407 sources, given that these units occupy only 13% and 7% of the surrounding area,  
50  
51 408 respectively. The importance of the marls as a source sediment, which outcrop only  
52  
53 409 to the north of the Ashkzar dunefield, suggests that net wind regime alone cannot be  
54  
55 410 considered as indicative of the net sediment transport in the region (Figure 1), as  
56  
57  
58  
59  
60

1  
2  
3 411 westerly winds are equally strong here yet import much less sediment. Both the wind  
4  
5 412 regime and potential sediment sources must be considered when evaluating net  
6  
7 413 aeolian sediment flux.  
8  
9

10 414 There is much spatial variation in the composition of the dune sands of Ashkzar erg  
11  
12 415 (Figure 6). Even before the geochemical composition of these sands is considered,  
13  
14 416 such variability is evident from the differing grain size profiles in the eight samples  
15  
16 417 investigated here (Table 1). Sample G, from the far south of the dunefield, contains  
17  
18 418 ~20% coarse sands (defined here as  $> 600 \mu\text{m}$ ), an unusually high figure for an  
19  
20 419 aeolian dune, although this sample is taken close to the border with the mapped  
21  
22 420 region of slipfaceless dome dunes, which tend to accumulate from coarser sands  
23  
24 421 (Lancaster, 1995). That said, sample H, from within the dome dunes, is not unusually  
25  
26 422 coarse.  
27  
28  
29

30  
31 423 Broadly, and considering the uncertainties presented by the methodology proposed  
32  
33 424 herein, two groups can be discerned within the samples geochemically analysed for  
34  
35 425 provenance (Figure 6). Samples taken from along the south and west of the  
36  
37 426 dunefield (B, E, F and G) are dominated to varying degrees by sediment from the  
38  
39 427 surrounding Quaternary fans and terraces (i.e. source unit Qt2), whereas most  
40  
41 428 samples to the north and east (A, D and H) show much greater contributions from  
42  
43 429 the Eocene marls (Egm) and clay flats (Qc). However, the division is not clear-cut;  
44  
45 430 sample C, in the northeast of the dunefield, has a dominant component from the Qt2  
46  
47 431 unit (with the second component only very slightly overlapped at  $2\sigma$  confidence  
48  
49 432 levels). It is, perhaps, unsurprising that the more northerly samples tend to show an  
50  
51 433 increased input from the Eocene marls (Egm), as these units have been shown to  
52  
53 434 contribute disproportionately to the sediment flux in the area, and also outcrop  
54  
55 435 exclusively on the northern side of the valley (Figure 1).  
56  
57  
58  
59  
60

1  
2  
3 436 The provenance of the sands is even less readily correlated with dune morphology,  
4  
5 437 with the Qt<sub>2</sub>-dominated sands occurring within three defined dune morphological  
6  
7 438 zones (barchans, barchanoid ridges and asymmetrical barchans). Samples A and B,  
8  
9 439 the closest pair of samples studied (~2.2 km apart), yield very different provenance  
10  
11 440 fingerprints, despite both lying within the region of Ashkzar erg dominated by  
12  
13 441 barchanoid ridges. The overall morphology of the dunes (Figure 3) supports spatially  
14  
15 442 and /or temporally variable sediment availability, with the transformation of barchans  
16  
17 443 to barchanoid ridges essentially being sediment-supply controlled, and asymmetric  
18  
19 444 barchan/linear forms believed to be the result of asymmetries of sediment supply, or  
20  
21 445 changes to the wind regime (Bagnold, 1941; Lancaster 1995).  
22  
23  
24  
25

26 446 The heterogeneity in the sediment provenance evident here suggests that either a)  
27  
28 447 some kind of fractionation of the aeolian sediment flux is occurring, with different  
29  
30 448 sources depositing sediment at different locations or b) different sediment transport  
31  
32 449 pathways have been active intermittently and asynchronously during the formation of  
33  
34 450 the dunefield. The similar physical composition (i.e. grain size) of the sources, and  
35  
36 451 the lack of evidence of systematic variation across the dunefield, would tend to  
37  
38 452 support the latter suggestion. Different sediment pathways might result from different  
39  
40 453 sources become more or less active over time, or might result from changing wind  
41  
42 454 regime over long (i.e. late Quaternary) timescales. The heterogeneity evident also  
43  
44 455 suggests that during dune accumulation periods, large-scale mixing of aeolian sands  
45  
46 456 from different sources (which might be expected given transport distances of 10-50  
47  
48 457 km) is not occurring. In the absence of any chronological control for these dunes,  
49  
50 458 such hypotheses cannot be conclusively tested currently, but establishing the  
51  
52 459 relative roles of spatial and temporal variability in dune accumulation would be a  
53  
54 460 worthwhile exercise.  
55  
56  
57  
58  
59  
60

1  
2  
3 461  
4  
56 462 **5. Conclusion**  
7

8  
9 463 In dryland environments, understanding the main sources for aeolian sediments is  
10  
11 464 an essential step in developing management strategies to reduce aeolian sediment  
12  
13 465 loadings and wind erosion. Establishing aeolian sediment pathways, however, is not  
14  
15 466 usually straightforward and is complicated when multiple potential source areas  
16  
17 467 might contribute to a region of net sand accumulation. The method proposed here,  
18  
19 468 based on methodologies applied to fluvial sediments, uses a suite of geochemical  
20  
21 469 data to identify the most apposite characteristics (the 'fingerprint') for discerning  
22  
23 470 superficially similar sources of aeolian sediment. Whereas these methods have  
24  
25 471 become widely adopted in fluvial geomorphology and catchment science over the  
26  
27 472 past two decades, they remain almost unused in aeolian science. Here, it has been  
28  
29 473 successfully demonstrated on fine sand in a small dunefield in central Iran, but it  
30  
31 474 might be applied equally to dust (i.e. silt) flux, although longer transport distances are  
32  
33 475 liable to prove more difficult to fingerprint unless relatively discrete and distinct  
34  
35 476 sources can be identified. The use of MCMC methods to provide confidence  
36  
37 477 estimates in the mixing model output enables more rigorous interpretation of the  
38  
39 478 relative importance of different sediment sources.  
40  
41  
42  
43  
44

45 479

46  
47 480 This method revealed within Ashkzar erg unexpected spatial heterogeneity of dune  
48  
49 481 composition (and thus provenance), which has a complex relationship with the  
50  
51 482 position within the dunefield, the dune type and other physical characteristics. The  
52  
53 483 Eocene marls in the surrounding area have been shown to contribute  
54  
55 484 disproportionately to the sediments of the dunes. In terms of management of sand  
56  
57 485 and dust hazard at this location, both the original source areas and those parts of the  
58  
59  
60

1  
2  
3 486 dunefield enriched in the Egm component might be viewed as priority targets for  
4  
5 487 landscape stabilization efforts, due to their apparent propensity for aeolian  
6  
7 488 mobilization.  
8

9  
10 489

11  
12 490 More widely, the methods proposed here for aeolian provenance unmixing method  
13  
14 491 can be applied to any mixed-source aeolian sediment to elucidate differing  
15  
16 492 susceptibilities to aeolian deflation, and reveal transport pathways at timescales  
17  
18 493 longer than those possible by either field study or remote sensing. Disciplines which  
19  
20 494 might benefit from the adoption of such methods include not just aeolian  
21  
22 495 geomorphology, but also dryland land management, soil science, engineering  
23  
24 496 geology and potentially palaeoenvironmental and palaeoclimatological studies. A  
25  
26 497 combination of the methods presented herein with geochronological studies may  
27  
28 498 enable calculation of flux rates to provide quantification of long-term sediment fluxes,  
29  
30 499 even when, as is very often the case with aeolian sediments, transport pathways are  
31  
32 500 complex and multi-phase.  
33  
34  
35

36 501

37  
38 502

### 39 40 503 **References**

41  
42  
43 504 Amiraslani, F. and Dragovich, D. (2011). Combating desertification in Iran over the  
44  
45 505 last 50 years: An overview of changing approaches. *Journal of Environmental*  
46  
47 506 *Management* 92 (1), 1-13. doi: 10.1016/j.jenvman.2010.08.012.  
48  
49

50  
51 507 Bagnold, R.A. 1941. The physics of blown sand. Methuen, London.  
52

53  
54 508 Box, G.E.P & Cox, D.R. (1964). An analysis of transformations. *Journal of the Royal*  
55  
56 509 *Statistical Society, Series B.* 26 (2): 211–252.  
57  
58  
59  
60



- 1  
2  
3 510 Brewer, M. J., Filipe, J. A. N., Elston, D. A., Dawson, L. A., Mayes, R. W., Soulsby,  
4  
5 511 Ch., & Dunn, S. M. (2005). A Hierarchical Model for Compositional Data  
6  
7 512 Analysis. *Journal of Agricultural, Biological, and Environmental Statistics*, 10(1),  
8  
9 513 19–34. doi:10.1198/108571105X28200
- 11  
12 514 Chen, F., Fang, N., & Shi, Z. (2016). Using biomarkers as fingerprint properties to  
13  
14 515 identify sediment sources in a small catchment. *Science of the Total*  
15  
16 516 *Environment*, 557-558, 123–133. doi:10.1016/j.scitotenv.2016.03.028
- 17  
18  
19  
20 517 Collins, A. L., & Walling, D. E. (2007). Sources of fine sediment recovered from the  
21  
22 518 channel bed of lowland groundwater-fed catchments in the UK. *Geomorphology*,  
23  
24 519 88, 120–138. doi:10.1016/j.geomorph.2006.10.018
- 25  
26  
27  
28 520 Collins, A. L., Zhang, Y., McChesney, D., Walling, D. E., Haley, S. M., & Smith, P.  
29  
30 521 (2012). Sediment source tracing in a lowland agricultural catchment in southern  
31  
32 522 England using a modified procedure combining statistical analysis and  
33  
34 523 numerical modelling. *Science of the Total Environment*, 414, 301–317.  
35  
36 524 doi:10.1016/j.scitotenv.2011.10.062
- 37  
38  
39 525 Collins, A. L., Zhang, Y. S., Duethmann, D., Walling, D. E., & Black, K. S. (2013).  
40  
41 526 Using a novel tracing-tracking framework to source fine-grained sediment loss to  
42  
43 527 watercourses at sub-catchment scale. *Hydrological Processes*, 27(6), 959–974.  
44  
45 528 doi:10.1002/hyp.9652
- 46  
47  
48  
49 529 Collins, A. L., Zhang, Y., Walling, D. E., Grenfell, S. E., & Smith, P. (2010). Tracing  
50  
51 530 sediment loss from eroding farm tracks using a geochemical fingerprinting  
52  
53 531 procedure combining local and genetic algorithm optimisation. *Science of the*  
54  
55 532 *Total Environment*, 408(22), 5461–5471. doi:10.1016/j.scitotenv.2010.07.066

- 1  
2  
3 533 Collins, A. L., Zhang, Y., Walling, D. E., Grenfell, S. E., Smith, P., Grischeff, J., ...  
4  
5 534 Brogden, D. (2012). Quantifying fine-grained sediment sources in the River Axe  
6  
7 535 catchment, southwest England: Application of a Monte Carlo numerical  
8  
9 536 modelling framework incorporating local and genetic algorithm optimisation.  
10  
11 537 *Hydrological Processes*, 26(13), 1962–1983. doi:10.1002/hyp.8283  
12  
13  
14 538 Collins, A.L., Pulley, S., Foster, I.D.L., Gellis A., Porto, P., Horowitz, A.J. (2016).  
15  
16 539 Sediment source fingerprinting as an aid to catchment management: A review of  
17  
18 540 the current state of knowledge and a methodological decision-tree for end-  
19  
20 541 users. *Journal of Environmental Management*, 194, 86–108.  
21  
22 542 doi.org/10.1016/j.jenvman.2016.09.075  
23  
24  
25 543 Cooper RJ and Krueger T (2017, in press). An extended Bayesian sediment  
26  
27 544 fingerprinting mixing model for the full Bayes treatment of geochemical  
28  
29 545 uncertainties. *Hydrological Processes*. DOI: 10.1002/hyp.11154.  
30  
31  
32  
33 546 Cooper, R. J., Krueger, T., Hiscock, K. M., & Rawlins, B. G. (2014). Sensitivity of  
34  
35 547 fluvial sediment source apportionment to mixing model assumptions: A  
36  
37 548 Bayesian model comparison. *Water Resources Research*, 9031–9047.  
38  
39 549 doi:10.1002/2014WR016194.  
40  
41  
42  
43 550 Cooper, R. J., Krueger, T., Hiscock, K. M., & Rawlins, B. G. (2015). High-temporal  
44  
45 551 resolution fluvial sediment source fingerprinting with uncertainty: A Bayesian  
46  
47 552 approach. *Earth Surface Processes and Landforms*, 40(1), 78–92.  
48  
49 553 doi:10.1002/esp.3621  
50  
51  
52  
53 554 Daga, R., Ribeiro Guevara, S., Sánchez, M. L., & Arribére, M. (2008). Source  
54  
55 555 identification of volcanic ashes by geochemical analysis of well preserved  
56  
57  
58  
59  
60

- 1  
2  
3 556 lacustrine tephras in Nahuel Huapi National Park. *Applied Radiation and*  
4  
5 557 *Isotopes*, 66(10), 1325–1336. doi:10.1016/j.apradiso.2008.03.009  
6  
7  
8 558 Defant, M.J. and Drummond, M.S. 1990. Derivation of some modern arc magmas by  
9  
10 559 melting of young subducted lithosphere. *Nature* 367, 662–665  
11  
12  
13 560 Delmonte, B., Baroni, C., Andersson, P.S., Schoberg, H., Hansson, M., Aciego, S.,  
14  
15 561 Petit, J.-R., Albani, S., Mazzola, C., Maggi, V., Frezzotti, M., 2010. Aeolian dust  
16  
17 562 in the Talos Dome ice core (East Antarctica, Pacific/Ross Sea sector): Victoria  
18  
19 563 Land versus remote sources over the last two climate cycles. *Journal of*  
20  
21 564 *Quaternary Science* 25, 1327-1337.  
22  
23  
24  
25 565 Delmonte, B., Basile-Doelsch, I., Petit, J.R., Maggi, V., Revel-Rolland, M., Michard,  
26  
27 566 A., Jagoutz, E., Grousset, F., 2004. Comparing the Epica and Vostok dust  
28  
29 567 records during the last 220,000 years: stratigraphical correlation and  
30  
31 568 provenance in glacial periods. *Earth-Science Reviews* 66, 63-87.  
32  
33  
34  
35 569 Dou, Y., Yang, S., Liu, Z., Clift, P. D., Shi, X., Yu, H., & Berne, S. (2010).  
36  
37 570 Provenance discrimination of siliciclastic sediments in the middle Okinawa  
38  
39 571 Trough since 30ka: Constraints from rare earth element compositions. *Marine*  
40  
41 572 *Geology*, 275(1-4), 212–220. doi:10.1016/j.margeo.2010.06.002  
42  
43  
44  
45 573 Douglas, G., Caitcheon, G., & Palmer, M. (2009). Sediment source identification and  
46  
47 574 residence times in the Maroochy River estuary, southeast Queensland,  
48  
49 575 Australia. *Environmental Geology*, 57(3), 629–639. doi:10.1007/s00254-008-  
50  
51 576 1336-7  
52  
53  
54 577 Egozcue, J. J., Pawlowsky-Glahn, V., Mateu-Figueras, G., & Barceló-Vidal, C.  
55  
56 578 (2003). Isometric Logratio Transformations for Compositional Data Analysis.  
57  
58  
59  
60

- 1  
2  
3 579 *Mathematical Geology*, 35(3), 279–300. doi:10.1023/A:1023818214614  
4  
5  
6 580 Fox, J. F., & Papanicolaou, A. N. (2008). An un-mixing model to study watershed  
7  
8 581 erosion processes. *Advances in Water Resources*, 31, 96–108.  
9  
10 582 doi:10.1016/j.advwatres.2007.06.008  
11  
12  
13 583 Garzanti, E., Vermeesch, P., Ando, S., Vezzoli, G., Valagussa, M., Allen, K., Kadi,  
14  
15 584 K.A., Al-Juboury, A.I.A., 2013. Provenance and recycling of Arabian desert  
16  
17 585 sand. *Earth-Science Reviews*. 120, 1-19.  
18  
19  
20  
21 586 Garzanti, E., Vermeesch, P., Padoan, M., Resentini, A., Vezzoli, G., Ando, S., 2014.  
22  
23 587 Provenance of Passive-Margin Sand (Southern Africa). *Journal of Geology*,  
24  
25 588 122(1), 17-42. doi:10.1086/674803  
26  
27  
28 589 Gellis, A. C., & Noe, G. B. (2013). Sediment source analysis in the Linganore Creek  
29  
30 590 watershed, Maryland, USA, using the sediment fingerprinting approach: 2008 to  
31  
32 591 2010. *Journal of Soils and Sediments*, 13(10), 1735–1753. doi:10.1007/s11368-  
33  
34 592 013-0771-6  
35  
36  
37  
38 593 Haddadchi, A, Ryder, D.S., Evrard, O., Olley, J. (2013). Sediment fingerprinting in  
39  
40 594 fluvial systems: review of tracers, sediment sources and mixing models. *Int. J.*  
41  
42 595 *Sediment Res.*, 28, 560–578  
43  
44  
45 596 Huntsman-Mapila, P., Kampunzu, A.B., Vink, B., Ringrose, S., 2005. Cryptic  
46  
47 597 indicators of provenance from the geochemistry of the Okavango Delta  
48  
49 598 sediments, Botswana. *Sedimentary Geology* 174, 123-148.  
50  
51  
52  
53 599 Honda, M., Yabuki, S., & Shimizu, H. S. H. I. (2004). Geochemical and isotopic  
54  
55 600 studies of aeolian sediments in China. *Sedimentology*, 211–230.  
56  
57 601 doi:10.1046/j.1365-3091.2003.00618.x  
58  
59  
60

- 1  
2  
3 602 Jia, Y., Fu, B., Jolivet, M. and Zheng, S. Cenozoic tectono-geomorphological growth  
4  
5 603 of the SW Chinese Tian Shan: insight from AFT and detrital zircon U-Pb data.  
6  
7 604 *Journal of Asian Earth Sciences*, 2015, 111, 395-413.  
8  
9  
10 605 Koiter, A. J., Owens, P. N., Petticrew, E. L., & Lobb, D. A. (2013). The behavioural  
11  
12 606 characteristics of sediment properties and their implications for sediment  
13  
14 607 fingerprinting as an approach for identifying sediment sources in river basins.  
15  
16 608 *Earth-Science Reviews*, 125, 24–42. doi:10.1016/j.earscirev.2013.05.009  
17  
18  
19  
20 609 Lancaster, N. 1995. *Geomorphology of Desert Dunes*. Routledge, London.  
21  
22  
23 610 Lin, J., Huang, Y., Wang, M. kuang, Jiang, F., Zhang, X., & Ge, H. (2015). Assessing  
24  
25 611 the sources of sediment transported in gully systems using a fingerprinting  
26  
27 612 approach: An example from South-east China. *Catena*, 129, 9–17.  
28  
29 613 doi:10.1016/j.catena.2015.02.012  
30  
31  
32  
33 614 Liu, B.L., Niu, Q.H., Qu, J.J., Zu, R.P. (2016). Quantifying the provenance of aeolian  
34  
35 615 sediments using multiple composite fingerprints. *Aeolian Research*, 22, 117-  
36  
37 616 122. doi:10.1016/j.aeolia.2016.08.002  
38  
39  
40 617 Lunn, D.J., Thomas, A., Best, N., and Spiegelhalter, D. (2000) WinBUGS -- a  
41  
42 618 Bayesian modelling framework: concepts, structure, and extensibility. *Statistics*  
43  
44 619 *and Computing*, 10:325--337.  
45  
46  
47  
48 620 Martínez-Carreras, N., Udelhoven, T., Krein, A., Gallart, F., Iffly, J. F., Ziebel, J. and  
49  
50 621 Walling, D. E. (2010). The use of sediment colour measured by diffuse  
51  
52 622 reflectance spectrometry to determine sediment sources: Application to the  
53  
54 623 Attert River catchment. *Journal of Hydrology*, 382(1-4), 49–63.  
55  
56 624 doi:10.1016/j.jhydrol.2009.12.017  
57  
58  
59  
60

- 1  
2  
3 625 Massoudieh, A., Gellis, A., Banks, W. S., & Wieczorek, M. E. (2013). Suspended  
4  
5 626 sediment source apportionment in Chesapeake Bay watershed using Bayesian  
6  
7 627 chemical mass balance receptor modeling. *Hydrological Processes*, 27(24),  
8  
9 628 3363–3374. doi:10.1002/hyp.9429  
10  
11  
12 629 Motha, J. A., Wallbrink, P. J., Hairsine, P. B., & Grayson, R. B. (2003). Determining  
13  
14 630 the sources of suspended sediment in a forested catchment in southeastern  
15  
16 631 Australia. *Water Resources Research*, 39(3), 1056. doi:10.1029/2001wr000794  
17  
18  
19  
20 632 Muhs, D. R., Lancaster, N. and Skipp, G.L. (2017). A complex origin for the Kelso  
21  
22 633 Dunes, Mojave National Preserve, California, USA: A case study using a simple  
23  
24 634 geochemical method with global applications. *Geomorphology*, 276, 222-243.  
25  
26 635 doi: 10.1016/j.geomorph.2016.10.002  
27  
28  
29  
30 636 Mukundan, R., Walling, D. E., Gellis, A. C., Slattery, M. C., & Radcliffe, D. E. (2012).  
31  
32 637 Sediment Source Fingerprinting: Transforming From a Research Tool to a  
33  
34 638 Management Tool. *Journal of the American Water Resources Association*,  
35  
36 639 48(6), 1241–1257. doi:10.1111/j.1752-1688.2012.00685.x  
37  
38  
39  
40 640 Naddafi, K., Nabizadeh, R., Soltanianzadeh, Z., Ehrampoosh, M.H., 2006.  
41  
42 641 Evaluation of dustfall in the air of Yazd. *Journal of Environmental Health*  
43  
44 642 *Science and Engineering*, 3, 161-168.  
45  
46  
47 643 Nanson, G.C., Chen, X.Y., Price, D.M. (1995). Aeolian and fluvial evidence of  
48  
49 644 changing climate and wind patterns during the past 100 Ka in the Western  
50  
51 645 Simpson Desert, Australia. *Palaeogeography Palaeoclimatology Palaeoecology*  
52  
53 646 113, 87-102.  
54  
55  
56  
57 647 Nie, J. and Peng, W. (2014). Automated SEM–EDS heavy mineral analysis reveals  
58  
59  
60

- 1  
2  
3 648 no provenance shift between glacial loess and interglacial paleosol on the  
4  
5 649 Chinese Loess Plateau. *Aeolian Research* 13, 71-75.  
6  
7  
8 650 Nosrati, K., Govers, G., Semmens, B. X., & Ward, E. J. (2014). A mixing model to  
9  
10 651 incorporate uncertainty in sediment fingerprinting. *Geoderma* 217-218, 173–180.  
11  
12 652 doi:10.1016/j.geoderma.2013.12.002  
13  
14  
15 653 Owens, P.N., Blake, W.H., Gaspar, L., Gateuille, D., Koiter, A.J., Lobb, D.A.,  
16  
17 654 Petticrew, E.L., Reiffarth, D.G., Smith, H.G. & Woodward, J.C. (2016).  
18  
19 655 Fingerprinting and tracing the sources of soils and sediments: Earth and ocean  
20  
21 656 science, geoarchaeological, forensic, and human health applications. *Earth-*  
22  
23 657 *Science Reviews*, 162, 1-23. doi: 10.1016/j.earscirev.2016.08.012  
24  
25  
26  
27 658 Palmer, M. J., & Douglas, G. B. (2008). A Bayesian statistical model for end member  
28  
29 659 analysis of sediment geochemistry, incorporating spatial dependences. *Journal*  
30  
31 660 *of the Royal Statistical Society. Series C: Applied Statistics* 57(3), 313–327.  
32  
33 661 doi:10.1111/j.1467-9876.2007.00615.x  
34  
35  
36  
37 662 Parnell, A. C., Phillips, D. L., Bearhop, S., Semmens, B. X., Ward, E. J., Moore, J.  
38  
39 663 W., Inger, R. (2013). Bayesian stable isotope mixing models. *Environmetrics*  
40  
41 664 24(6), 387–399. doi:10.1002/env.2221  
42  
43  
44  
45 665 Pell, S.D., Williams, I.S., Chivas, A.R., 1997. The use of protolith zircon-age  
46  
47 666 fingerprints in determining the protosource areas for some Australian dune  
48  
49 667 sands. *Sedimentary Geology* 109, 233-260.  
50  
51  
52 668 Pell, S.D., Chivas, A.R., Williams, I.S. 2000. The Simpson, Strzelecki and Tirari  
53  
54 669 Deserts: development and sand provenance. *Sedimentary Geology* 130 (1-2),  
55  
56 670 107–130. doi: 10.1016/S0037-0738(99)00108-6  
57  
58  
59  
60

- 1  
2  
3 671 Pethierick, L., McGowan, H., Moss, P., 2008. Climate variability during the Last  
4  
5 672 Glacial Maximum in eastern Australia: evidence of two stadials? *Journal of*  
6  
7 673 *Quaternary Science* 23, 787-802.
- 8  
9  
10 674 Pittam, N. J., Foster, I. D. L., & Mighall, T. M. (2009). An integrated lake-catchment  
11  
12 675 approach for determining sediment source changes at Aqualate Mere, Central  
13  
14 676 England. *Journal of Paleolimnology*, 42(2), 215–232. doi:10.1007/s10933-008-  
15  
16 677 9272-9
- 17  
18  
19  
20 678 Rao, W., Tan, H., Jiang, S., & Chen, J. (2011). Trace element and REE  
21  
22 679 geochemistry of fine- and coarse-grained sands in the Ordos deserts and links  
23  
24 680 with sediments in surrounding areas. *Chemie Der Erde - Geochemistry*, 71(2),  
25  
26 681 155–170. doi:10.1016/j.chemer.2011.02.003
- 27  
28  
29  
30 682 Ren, R., Han, B-F., Xu, Z. and Li, Q. 2014. When did the subduction first initiate in  
31  
32 683 the southern Paleo-Asian Ocean: New constraints from a Cambrian intra-  
33  
34 684 oceanic arc system in West Junggar, NW China. *Earth and Planetary Science*  
35  
36 685 *Letters* 388, 222–236
- 37  
38  
39 686 Semmens, B. X., Moore, J. W., & Ward, E. J. (2009). Improving Bayesian isotope  
40  
41 687 mixing models: A response to Jackson et al. (2009). *Ecology Letters*, 12(3), 10–  
42  
43 688 12. doi:10.1111/j.1461-0248.2009.01283.x
- 44  
45  
46  
47 689 Sherriff, S. C., Franks, S. W., Rowan, J. S., Fenton, O., & Ó'hUallacháin, D. (2015).  
48  
49 690 Uncertainty-based assessment of tracer selection, tracer non-conservativeness  
50  
51 691 and multiple solutions in sediment fingerprinting using synthetic and field data.  
52  
53 692 *Journal of Soils and Sediments*, 15(10), 2101–2116. doi:10.1007/s11368-015-  
54  
55 693 1123-5



- 1  
2  
3 694 Smith, H. G., & Blake, W. H. (2014). Sediment fingerprinting in agricultural  
4  
5 695 catchments: A critical re-examination of source discrimination and data  
6  
7 696 corrections. *Geomorphology*, 204, 177–191.  
8  
9  
10 697 doi:10.1016/j.geomorph.2013.08.003  
11  
12  
13 698 Stewart, H. A., Massoudieh, A., & Gellis, A. (2015). Sediment source apportionment  
14  
15 699 in Laurel Hill Creek, PA, using Bayesian chemical mass balance and isotope  
16  
17 700 fingerprinting. *Hydrological Processes*, 29(11), 2545–2560.  
18  
19 701 doi:10.1002/hyp.10364  
20  
21  
22 702 Stone, M., Collins, A. L., Silins, U., Emelko, M. B., & Zhang, Y. S. (2014). The use of  
23  
24 703 composite fingerprints to quantify sediment sources in a wildfire impacted  
25  
26 704 landscape, Alberta, Canada. *Science of the Total Environment*, 473-474, 642–  
27  
28 705 650. doi:10.1016/j.scitotenv.2013.12.052  
29  
30  
31  
32 706 Thorpe, R.I., Hickman, A.H., Davis, D.W., Mortensen, J.K. and Trendall, A.F., 1992.  
33  
34 707 U/Pb zircon geochronology of Archaean felsic units in the Marble Bar region,  
35  
36 708 Pilbara Craton, Western Australia. *Precambrian Research*, 56, 169-189.  
37  
38  
39 709 Vale, S. S., Fuller, I. C., Procter, J. N., Basher, L. R., & Smith, I. E. (2016).  
40  
41 710 Characterization and quantification of suspended sediment sources to the  
42  
43 711 Manawatu River, New Zealand. *Science of The Total Environment*, 543, 171–  
44  
45 712 186. doi:10.1016/j.scitotenv.2015.11.003  
46  
47  
48  
49 713 Voli, M. T., Wegmann, K. W., Bohnenstiehl, D. R., Leithold, E., Osburn, C. L., &  
50  
51 714 Polyakov, V. 2013. Fingerprinting the sources of suspended sediment delivery  
52  
53 715 to a large municipal drinking water reservoir: Falls Lake, Neuse River, North  
54  
55 716 Carolina, USA. *Journal of Soils and Sediments*, 13(10), 1692–1707.  
56  
57  
58  
59  
60

- 1  
2  
3 717 doi:10.1007/s11368-013-0758-3  
4  
5  
6 718 Walling, D.E., Collins, A.L., & Stroud, R.W. 2008. Tracing suspended sediment and  
7  
8 719 particulate phosphorus sources in catchments. *Journal of Hydrology*, 350(3-4),  
9  
10 720 274–289. doi:10.1016/j.jhydrol.2007.10.047  
11  
12  
13 721 Walling, D.E. 2013. The evolution of sediment source fingerprinting investigations in  
14  
15 722 fluvial systems. *Journal of Soils and Sediments*, 13(10), 1658-1675. doi:  
16  
17 723 10.1007/s11368-013-0767-2  
18  
19  
20  
21 724 Wasklewicz, T.A., Meek, N., 1995. Provenance of aeolian sediment: The upper  
22  
23 725 Coachella Valley, California. *Physical Geography* 16, 539-556.  
24  
25  
26 726 Wilkinson, S.N., Hancock, G.J., Bartley, R., Hawdon, A.A., & Keen, R.J. (2013).  
27  
28 727 Using sediment tracing to assess processes and spatial patterns of erosion in  
29  
30 728 grazed rangelands, Burdekin River basin, Australia. *Agriculture, Ecosystems*  
31  
32 729 *and Environment*, 180, 90–102. doi:10.1016/j.agee.2012.02.002  
33  
34  
35  
36 730 Wilson, C.G., Papanicolaou, A.N.T., & Denn, K.D. (2012). Partitioning fine sediment  
37  
38 731 loads in a headwater system with intensive agriculture. *Journal of Soils and*  
39  
40 732 *Sediments*, 12(6), 966–981. doi:10.1007/s11368-012-0504-2  
41  
42  
43 733 Winspear, N.R., Pye, K., 1996. Textural, geochemical and mineralogical evidence for  
44  
45 734 the sources of aeolian sand in central and southwestern Nebraska, USA.  
46  
47 735 *Sedimentary Geology* 101, 85-98.  
48  
49  
50  
51 736 Yang, X., Liu, Y., Li, C., Song, Y., Zhu, H., Jin, X., 2007. Rare earth elements of  
52  
53 737 aeolian deposits in Northern China and their implications for determining the  
54  
55 738 provenance of dust storms in Beijing. *Geomorphology* 87, 365-377.  
56  
57  
58  
59  
60

1  
2  
3 739  
4  
5  
6 740  
7  
8  
9 741  
10  
11  
12  
13  
14  
15  
16  
17  
18  
19  
20  
21  
22  
23  
24  
25  
26  
27  
28  
29  
30  
31  
32  
33  
34  
35  
36  
37  
38  
39  
40  
41  
42  
43  
44  
45  
46  
47  
48  
49  
50  
51  
52  
53  
54  
55  
56  
57  
58  
59  
60

For Peer Review

742 Tables

743 Table 1

	Grain size ( $\mu\text{m}$ )						
	<62.5	62.5 - 150	150 - 300	300 - 600	600 - 1180	1180 - 1700	
Mean Eocene marl (Egm) source (% $\pm 1\sigma$ )	3.0 $\pm$ 1.4	40.2 $\pm$ 10.6	20.0 $\pm$ 6	15.1 $\pm$ 4.2	15.6 $\pm$ 6.7	6.1 $\pm$ 5	
Mean Quaternary clay flat (Qc) source (% $\pm 1\sigma$ )	3.1 $\pm$ 1.3	29.4 $\pm$ 9.2	21.8 $\pm$ 5.6	19.0 $\pm$ 3.9	19.7 $\pm$ 8.1	6.9 $\pm$ 4	
Mean Quaternary terrace/fan (Qt2) source (% $\pm 1\sigma$ )	2.2 $\pm$ 2.3	34.7 $\pm$ 7.3	20.4 $\pm$ 5.6	17.1 $\pm$ 3.9	19.3 $\pm$ 5.3	6.4 $\pm$ 2	
Mean Ashkzar erg dune sands (% $\pm$ 1 $\sigma$ )	1.1 $\pm$ 0.9	47.8 $\pm$ 9.3	29.7 $\pm$ 8.4	17.4 $\pm$ 13.9	3.4 $\pm$ 5.4	0.6 $\pm$ 1.3	
Ashkzar erg dune samples (%)	A	0.3	57.6	38.2	3.4	0.5	0.0
	B	0.5	41.0	18.1	39.0	1.4	0.0
	C	2.1	43.9	16.7	35.9	1.4	0.0
	D	0.5	42.5	34.0	22.0	1.0	0.0
	E	2.7	51.8	31.2	7.9	5.0	1.4
	F	1.0	64.5	32.0	2.5	0.0	0.0
	G	1.0	36.8	28.0	14.4	16.2	3.6
	H	0.6	44.6	39.3	13.7	1.8	0.0

744

745 Table 2

Fingerprint property	Chi square	p value	Fingerprint property	Chi square	p-value
La	6.669	0.036*	Y	4.151	0.125
Ce	7.476	0.024**	Zr	3.744	0.154
Pr	9.552	0.008**	Nb	0.582	0.748
Nd	0.415	0.813	Hf	16.1	<0.001***
Sm	0.081	0.96	Ta	4.922	0.085
Eu	10.23	0.006**	Th	10.28	0.006**
Gd	0.434	0.805	U	4.8	0.091
Tb	0.017	0.992	As	5.166	0.076
Dy	1.359	0.507	Bi	0.725	0.695
Ho	8.067	0.018*	Cd	0.111	0.946
Er	9.257	0.01*	Ga	13.4	<0.001***
Tm	8.373	0.015*	Ge	0.59	0.745
Yb	1.026	0.599	In	1.215	0.545
Lu	0.104	0.949	Li	7.213	0.027*
ΣREE	7.086	0.029*	Mo	0.227	0.893
Eu/Eu*	10.23	0.006**	P	13.05	<0.001***
(Nd/Yb)	0.785	0.675	S	16.36	<0.001***
(Gd/Yb) <sub>n</sub>	0.729	0.695	Sb	1.409	0.494
(La/Yb) <sub>n</sub>	13.89	0.001**	Se	0.858	0.651
(La/Sm) <sub>n</sub>	4.725	0.094**	Sn	6.466	0.039*
(La/Lu) <sub>n</sub>	12.78	0.002**	Te	4.685	0.096
δCe	5.435	0.041***	Ti	6.56	0.038*
Rb	15.18	<0.001***	Tl	6.614	0.037*
Sr	16.44	<0.001***	W	0.086	0.958
Ba	6.379	0.041*	Mn	1.673	0.433
V	3.083	0.214	Si	0.342	0.843
Cr	5.359	0.069	<sup>143</sup> Nd	1.042	0.534
Co	1.271	0.53	<sup>144</sup> Nd	2.031	0.362
Ni	3.998	0.135	<sup>86</sup> Sr	5.754	0.056
Cu	3.18	0.204	<sup>87</sup> Sr	7.124	0.028*
Zn	0.236	0.889			

746

747 Table 3

Sediment	Tracer	Optimum composite fingerprints					
		Rb	Sr	<sup>87</sup> Sr	(La/Yb) <sub>n</sub>	Ga	δCe
Sand dune	Mean	7.8	144	85	7.1	1.2	0.69
	SD	0.74	18.6	28	0.54	0.11	0.020
Source	Tracer	Rb	Sr	<sup>87</sup> Sr	(La/Yb) <sub>n</sub>	Ga	δCe
Egm	Mean	8.9	293	82	6.9	1.3	0.70
	SD	2.3	192	31	0.58	0.29	0.085
Qc	Mean	10	139	91	7.4	1.1	0.69
	SD	2.6	36.5	31	0.54	0.27	0.071
Qt2	Mean	7.1	163	98	7.7	0.99	0.74
	SD	0.82	135	44	0.89	0.26	0.27

748

749 Table 4

	Source	Tracer					
		Rb	Sr	<sup>87</sup> Sr	(La/Yb) <sub>n</sub>	Ga	δCe
Raw data	Egm	0.944	0.362	0.930	0.996	0.980	0.810
	Qc	0.347	0.734	0.486	0.794	0.900	0.167
	Qt2	0.983	0.019	0.182	0.557	0.710	0.013
	Source	Tracer					
		Rb	Sr	<sup>87</sup> Sr	(La/Yb) <sub>n</sub>	Ga	δCe
Box-Cox transformed data	Egm	0.944	0.724	0.930	0.996	0.980	0.978
	Qc	0.347	0.931	0.486	0.794	0.900	0.542
	Qt2	0.983	0.085	0.182	0.557	0.710	0.061

750

751 Table 5

752

Sediment samples	Source	Mean (%)	SD (%)	MC error	Median	Percentile (2.5)	Percentile (97.5)
A	Egm	44.1	11.5	0.003	44.5	21	64.7
	Qc	39.8	11.2	0.003	37.9	22.7	65.8
	Qt2	16.2	8.3	0.001	15.2	3.6	34
B	Egm	32.6	7.3	0.002	33	18.2	46.2
	Qc	5.1	3.8	0.001	4.1	0.6	15
	Qt2	62.2	6	0.001	62.1	50.3	73.7
C	Egm	20.8	6.3	0.002	21	8.1	33
	Qc	27.5	6.5	0.002	26.6	17.1	43
	Qt2	51.6	5.2	0.000	51.1	42	62.5
D	Egm	56.3	13	0.004	56.9	29.9	79.4
	Qc	28.7	10.5	0.003	27	12.2	53.4
	Qt2	14.9	9.4	0.001	14.4	0.4	34.2
E	Egm	14.3	5	0.001	14.3	4.6	24.6

		Qc	23	5.3	0.001	22.3	14.2	35.1
		Qt2	62.6	4.8	0.000	62.7	52	71.9
	F	Egm	17.6	6.3	0.001	17.7	4.8	29.9
		Qc	32.4	7.4	0.002	31.5	20.4	49.6
		Qt2	49.9	5.5	0.001	49.4	39.7	61.5
	G	Egm	3.4	3.2	0.000	2.44	0.000	12.2
		Qc	3.9	3.9	0.000	2.6	0.000	14.7
		Qt2	92.7	6	0.001	94	78.2	99.7
	H	Egm	37.3	11.2	0.003	37.8	14.5	57.9
		Qc	49.7	12.6	0.004	47.7	30	79
		Qt2	13	8.6	0.001	12	0.4	31.5

753

754

For Peer Review

1  
2  
3  
4  
5  
6  
7  
8  
9  
10  
11  
12  
13  
14  
15  
16  
17  
18  
19  
20  
21  
22  
23  
24  
25  
26  
27  
28  
29  
30  
31  
32  
33  
34  
35  
36  
37  
38  
39  
40  
41  
42  
43  
44  
45  
46  
47  
48  
49  
50  
51  
52  
53  
54  
55  
56  
57  
58  
59  
60

1  
2  
3 755 Figure captions  
4  
5

6 756  
7

8 757 *Figure 1: Location and geological map of the Yazd-Ardekan Plain and sampling*  
9  
10 758 *sites. Dominant and minor wind directions shown in Part C. Number of sampling*  
11  
12 759 *points = 57. Qt2, Qc, Egm (potential sediment sources) and Qsd (sediment)*  
13  
14 760 *represent young alluvial fans and terraces, clay flats, gypsiferous marl and sand*  
15  
16 761 *dunes, respectively.*  
17  
18

19 762  
20

21 763 *Figure 2: Source and sediment sink regions within the study area. Source regions*  
22  
23 764 *include: a) clay flats (Qc); b) gypsiferous marl (Egm); and c) young alluvial fans and*  
24  
25 765 *terraces (Qt2). Sediment sinks include: d) sand dunes (Qsd).*  
26  
27

28 766  
29

30 767 *Figure 3. Morphological mapping of dune types within Ashkzar erg reveals the*  
31  
32 768 *dominance of barchans and barchanoid ridges. There are less distinct zones within*  
33  
34 769 *the dunefield in the north, where the interdunes are sandy and the transverse forms*  
35  
36 770 *much less distinct, and in the far southeast, where patchy slipface-less dunes*  
37  
38 771 *dominate. Base imagery is courtesy of Google Earth™, and letters refer to the eight*  
39  
40 772 *samples analysed for physical and geochemical characteristics within the dunefield.*  
41  
42

43 773  
44

45 774 *Figure 4: A directed acyclic graph of the Bayesian mixing model employed in this*  
46  
47 775 *study.*  
48

49 776  
50

51  
52 777 *Figure 5: Two-dimensional scatter plot of the first and second discriminant functions*  
53  
54 778 *from stepwise DFA for the source groups Egm (Eocene gypsiferous marls), Qc*  
55  
56 779 *(Quaternary clay flats) and Qt2 (Quaternary alluvial fans and terraces).*  
57  
58  
59  
60



1  
2  
3 780 *Figure 6: Source contributions for each aeolian sediment samples by Bayesian*  
4  
5 781 *mixing model with 95% credible limits. Base imagery is courtesy of Google Earth™.*  
6  
7

8 782  
9

10  
11 783 Table captions  
12

13  
14 784 *Table 1: Grain size data for the source areas, the dunefield, and individual samples*  
15  
16 785 *from within the dunefield.*  
17

18 786  
19

20  
21 787 *Table 2: Kruskal-Wallis H test results for selecting fingerprint properties for*  
22  
23 788 *distinguishing individual source types. Confidence is highlighted at >95% with a*  
24  
25 789 *single asterisk, >99% with a double asterisk, and >99.9% with a triple asterisk.*  
26

27 790  
28

29  
30 791 *Table 3: Summary geochemistry data for sand dune samples and potential sediment*  
31  
32 792 *sources. All are reported to two significant figures, except Sr, which is reported to*  
33  
34 793 *three, due to the larger magnitude of the concentrations.*  
35

36 794  
37

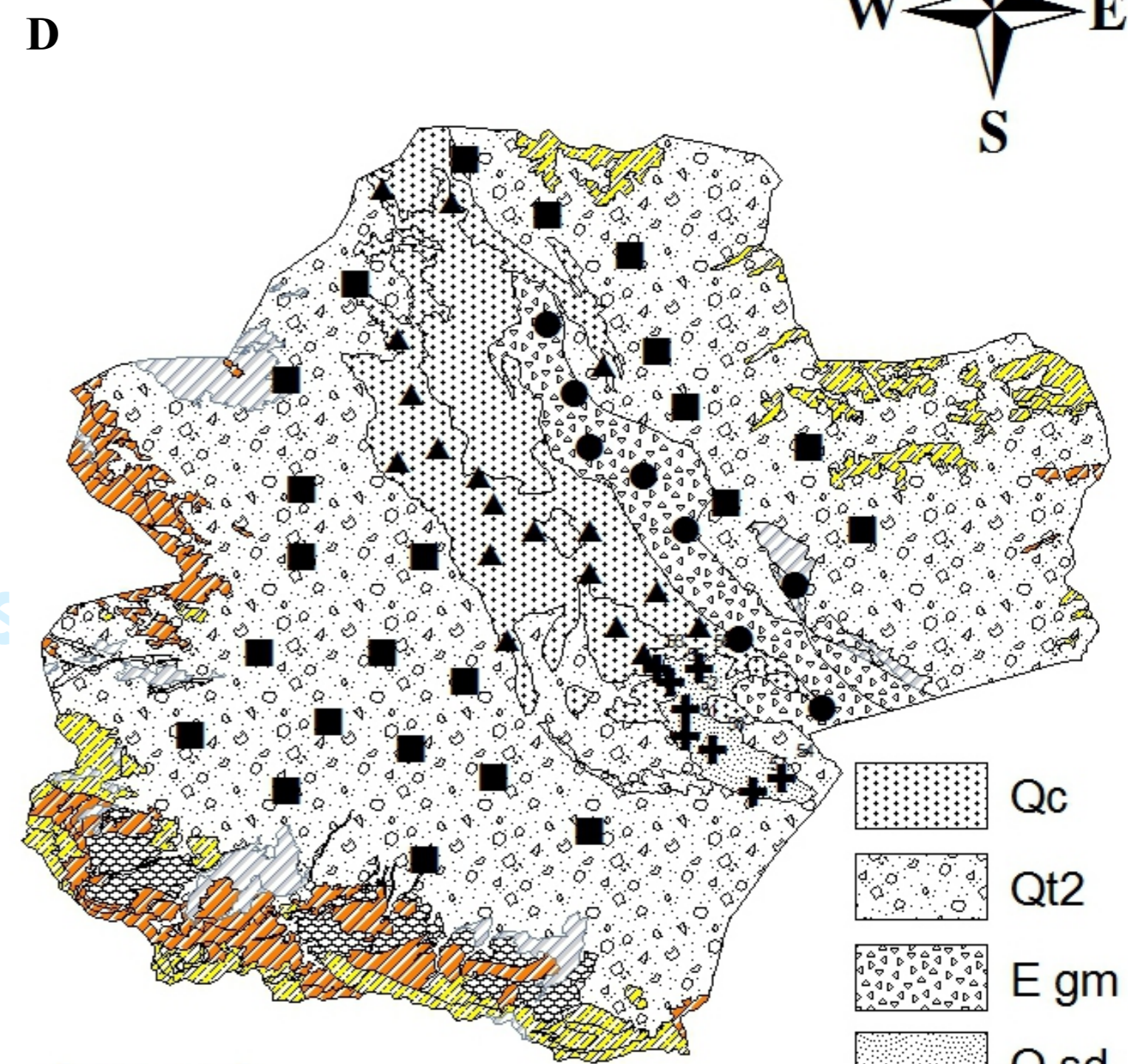
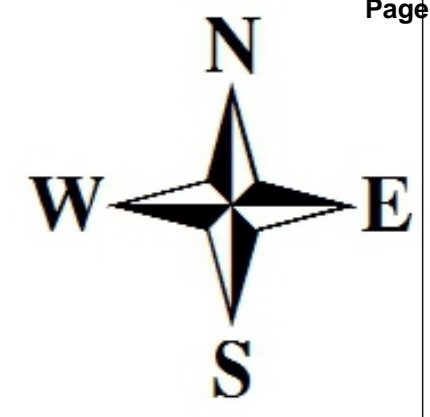
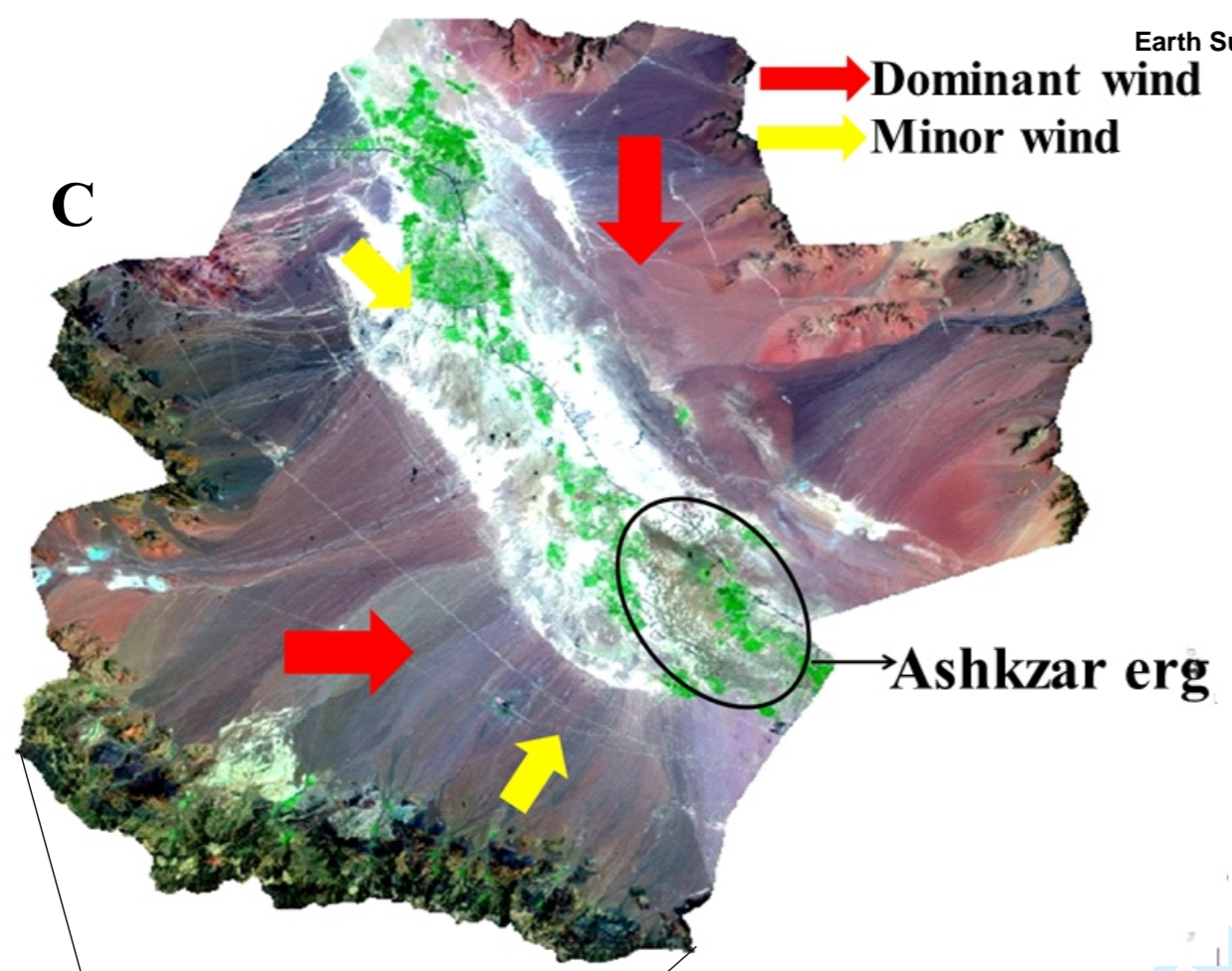
38  
39 795 *Table 4: Normality tests on the raw data for the tracers selected for the fingerprint*  
40  
41 796 *revealed that two tracers (Sr and  $\delta^{13}C$ ) were not normally distributed for the Qt2 unit;*  
42  
43 797 *for this reason, Box-Cox transformations were performed on all data, which did*  
44  
45 798 *provide normal distributions for all tracers.*  
46

47 799  
48

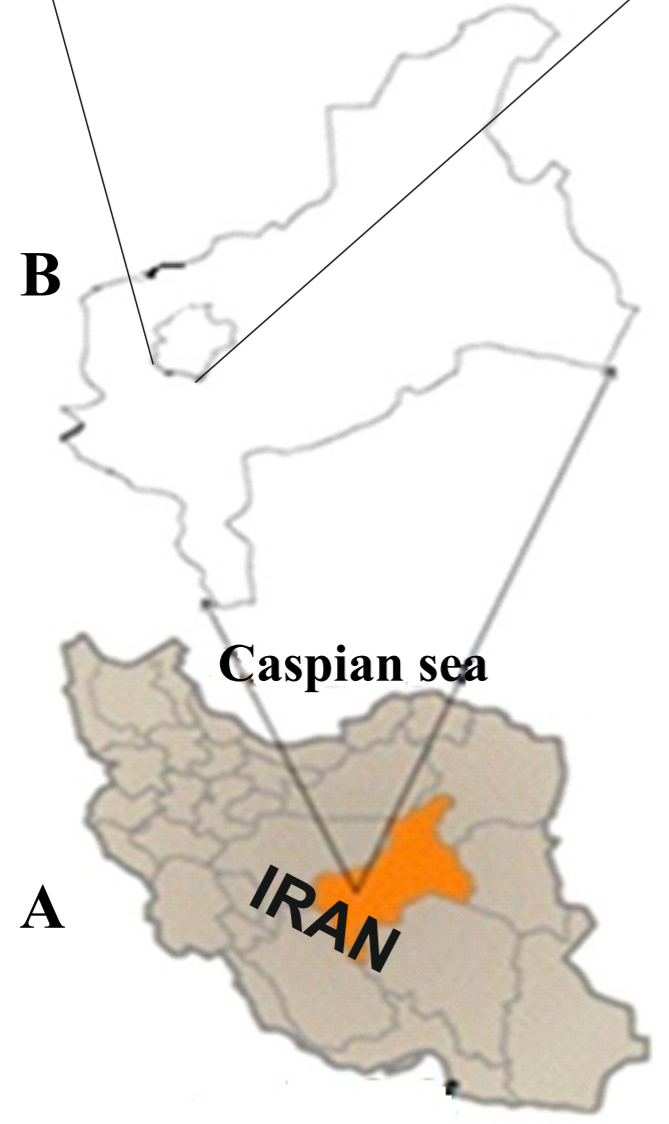
49  
50 800 *Table 5. Estimated contribution from each source for aeolian sediment samples by*  
51  
52 801 *Bayesian mixing model.*  
53

54 802  
55

56 803  
57  
58  
59  
60



**A.** Iran map  
**B.** Yazd Province boundary  
**C.** Satellite image of Yazd-Ardekan Plain  
**D.** Geological map of Yazd-Ardekan Plain

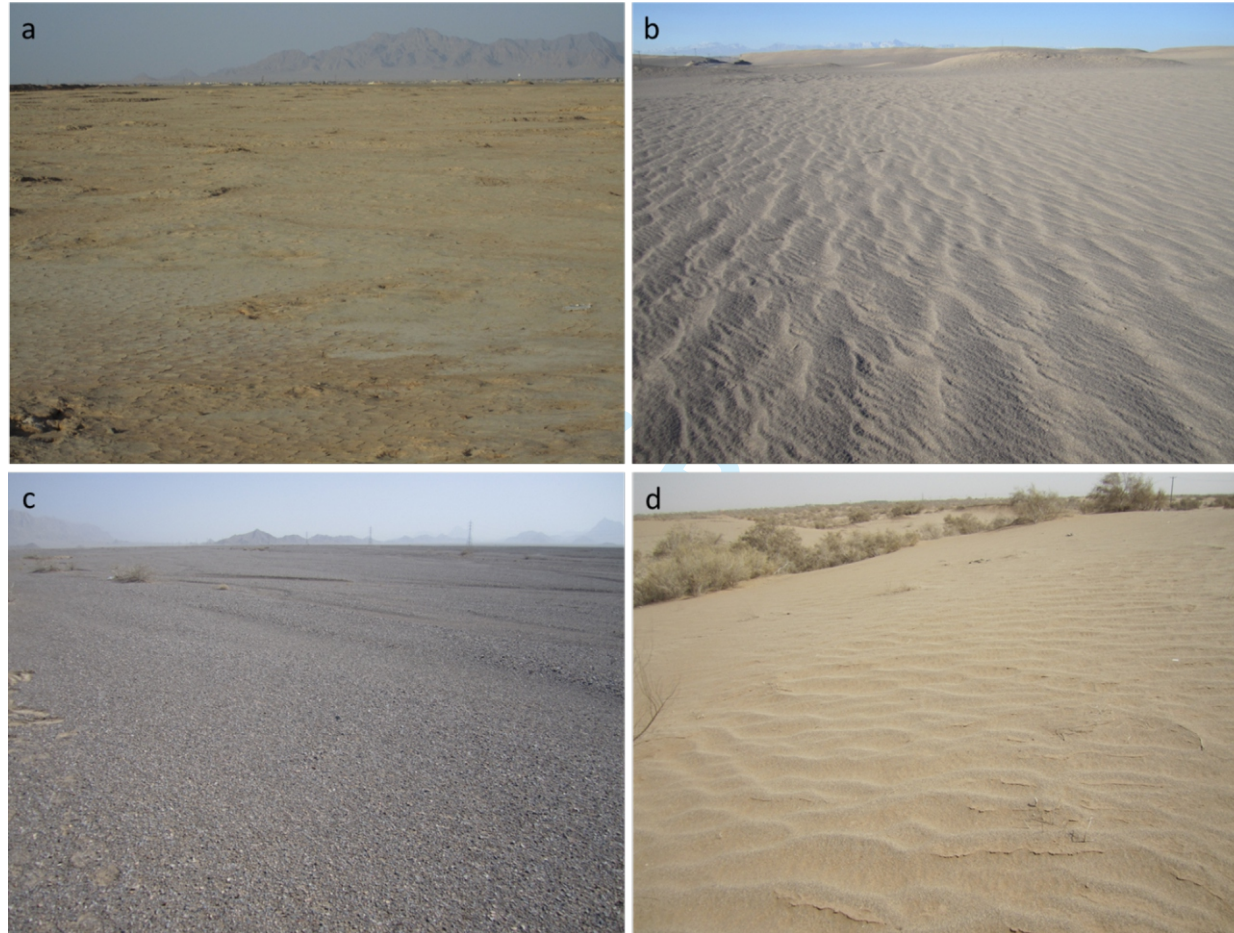


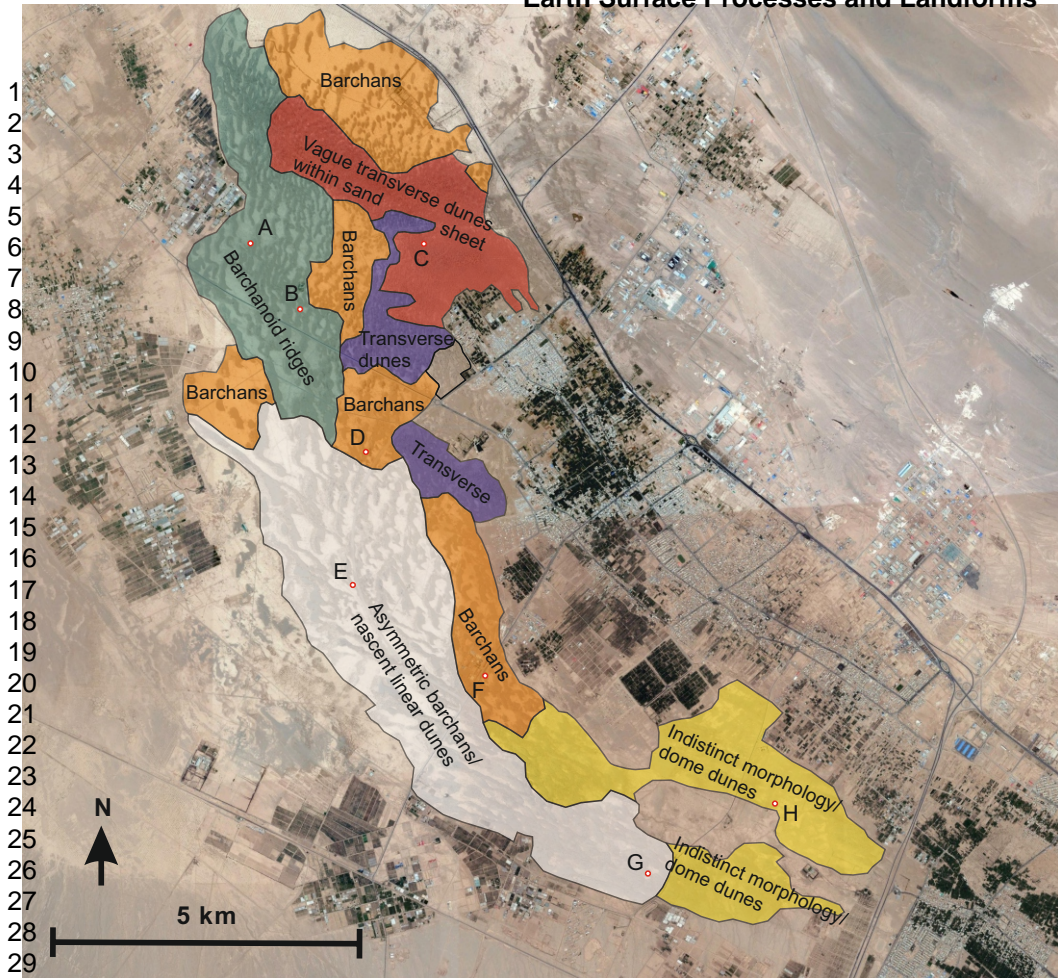
**Legend**

- Egm sample
- Qt2 sample
- ▲ Qc sample
- ✚ Sand dune sample
- ▨ Paleozoic Formations
- ▧ Cenozoic Formations
- ▩ Mesozoic Formations
- ▤ Pre-Cambrian Formations
- ▧ Qc
- ▨ Qt2
- ▩ E gm
- ▤ Q sd

1  
2  
3  
4  
5  
6  
7  
8  
9  
10  
11  
12  
13  
14  
15  
16  
17  
18  
19  
20  
21  
22  
23  
24  
25  
26  
27  
28  
29  
30  
31  
32  
33  
34  
35  
36  
37  
38  
39  
40  
41  
42  
43  
44  
45  
46  
47  
48  
49  
50  
51  
52  
53  
54  
55  
56  
57  
58  
59  
60

1  
2  
3  
4  
5  
6  
7  
8  
9  
10  
11  
12  
13  
14  
15  
16  
17  
18  
19  
20  
21  
22  
23  
24  
25  
26  
27  
28  
29  
30  
31  
32  
33  
34  
35  
36  
37  
38  
39  
40  
41  
42  
43  
44  
45  
46  
47





Peer Review

1  
2  
3  
4  
5  
6  
7  
8  
9  
10  
11  
12  
13  
14  
15  
16  
17  
18  
19  
20  
21  
22  
23  
24  
25  
26  
27  
28  
29  
30  
31  
32  
33  
34  
35  
36  
37  
38  
39  
40  
41  
42  
43  
44  
45  
46  
47  
48  
49  
50  
51  
52  
53  
54  
55  
56  
57  
58  
59  
60

**Source**

**Contribution**

**Sediment**

